Desalination and Water Treatment
www.deswater.com

doi: 10.5004/dwt.2022.29035

277 (2022) 266–275
November

Linear and nonlinear isotherm, kinetic and thermodynamic behavior of benzene adsorption using sodium dodecyl sulfate functionalized magnetic nanoparticle adsorbent

Ferdos Kord Mostafapour[a], Neda Jabari[b], Morteza Khodadadi Saloot[c], Aram Dokht Khatibi[a], Hossein Moein[a], Davoud Balarak[a,*]

[a]*Department of Environmental Health, Health Promotion Research Center, Zahedan University of Medical Sciences, Zahedan, Iran, email: dbalarak2@gmail.com (D. Balarak)*
[b]*Student Research Committee, Zahedan University of Medical Sciences, Zahedan, Iran*
[c]*Department of Environmental Engineering, Faculty of Natural Resources and Environment, Science and Research Branch, Islamic Azad University, Tehran, Iran*

Received 15 June 2022; Accepted 12 October 2022

ABSTRACT

In this study, magnetic nanoparticles (MNs) were modified by sodium dodecyl sulfate (SDS) and used to remove benzene from aqueous solutions. The adsorbent in the study was named MNs/SDS. To determine the adsorbent properties of the adsorbent, Fourier-transform infrared spectroscopy, scanning electron microscopy, X-ray diffraction, and Brunauer–Emmett–Teller tests were used. The results showed that the pH of 7, the adsorbent dose of 0.6 g/L, the concentration of 10 mg/L, the contact time of 60 min, and the temperature of 50°C were the best conditions, and all initial benzene concentration was lost. Linear and nonlinear isotherm and kinetics models were calculated. The results showed that the equilibrium data follow the Langmuir isotherm, which represents the monolayer adsorption of the pollutant, and the pseudo-second-order kinetics is also used for the rate of the reactions. Using the Dubinin–Radushkevich isotherm model and average adsorption energy, it can be proved that adsorption at all temperatures is a physical process. Maximum adsorption capacity, according to the Langmuir model at 20°C, 30°C, 40°C, and 50°C, was 127, 131.2, 139.6, and 140.4 mg/g. Also, negative Gibbs free energy values and positive enthalpy and entropy values indicate that the reaction is spontaneous and endothermic, and randomly during the adsorption process.

Keywords: Thermodynamics; Adsorption equilibrium; Benzene; Modified magnetic nanoparticles; Sodium dodecyl sulfate

1. Introduction

The bottlenecks caused by population growth and pressure on water resources have necessitated the protection of these resources [1,2]. The development of exploration, extraction, and exploitation of oil resources in oil-rich countries has caused many environmental problems for those countries [3]. One of the most important problems is the pollution of water resources and the increase in the amount of hydrocarbons in the water. Numerous organic compounds that are entered into the oil and petrochemical industries and their downstream industries are resistant to biodegradation and have the potential for toxicity to humans [4]. Treatment of these compounds in biological treatment processes is usually difficult, and they are called refractory compounds. A compound that is present

* Corresponding author.

in the effluents of the above-mentioned industries is benzene (C_6H_6) [5,6]; it is employed in large quantities as a solvent in the chemical industry as well as a raw material or intermediate in the synthesis of a number of chemicals (such as styrene, phenol, aniline) [7]. It has been known as the smallest and most stable aromatic compound, which is a colorless and clear liquid with an aromatic odor that is among the features of aromatic compounds [8]. It has also been found to be highly inflammable [9]. Inhalation of high levels of benzene vapors can cause drowsiness, dizziness, nausea, and headaches. Much higher concentrations or longer contact times have been observed to be associated with seizures, loss of consciousness, and eventually death [10,11]. However, the most important effect of long-term contact with it is the adverse effect on the blood. Benzene damages the bone marrow and leads to anemia by reducing red blood cells. It can also cause bleeding and weaken the immune system, which increases the risk of infection [12,13]. In addition, due to the biological oxidizing properties of this compound in the body and the formation of epoxy, benzene is carcinogenic [14,15]; so that, it has been classified as a primary pollutant by the Environmental Protection Agency (EPA) and Group A carcinogens (with definite carcinogenicity). Above-mentioned health issues have led to determining the allowable value of 0.5 μg/L for this compound by EPA [16,17].

The above-mentioned information indicates the importance of attempts for introducing effective methods to employ for removing benzene from water and wastewaters; accordingly, the techniques including coagulation, precipitation, filtration, irradiation, adsorption on activated carbon, and use of other adsorbents were evaluated to remove petroleum and aromatic compounds [18,19]. The results of the studies conducted by employing mentioned methods were indicative of superior appropriateness of the adsorption for removal of these types of pollutants; researchers of adsorption studies have reported that method is simple and convenient in design and operation and is able to offer high efficiency in removal of pollutants [20,21]. However, the adsorbent, which is commercially available and employed as the best adsorbent, that is, activated carbon, has represented difficulties in regeneration and separation from the solutions. Thus, studies have continued to introduce new adsorbents without mentioned issues [22,23].

One of these studied adsorbents in recent decades is nanoparticles, for example, magnetic nanoparticles (MNs); this adsorbent has found remarkable popularity since its surface to volume ratio is high, and it has numerous vacant active sites, which develops the separating and removing the pollutants from solutions [24–26]. Moreover, MNs have magnetic properties, which facilitate their separation without the need for centrifugation and filtration and provide a better condition for their reuse [27–29]. Despite the mentioned benefits, the agglomeration of this adsorbent, which is attributed to a reduction in surface energy and leads to decreasing surface areas and adsorption efficiency, exhibits the need for conducting modification of it to solve the mentioned problem. The use of sodium dodecyl sulfate (SDS) for the modification of MNs is one of the solutions, which has been the subject of different studies; so that this has led to solving the problem and enhancing the effectiveness of adsorption by MNs [30]. In the conducted studies, effective binding and chelating of functional groups present in SDS with the surface of MNs have been reported to be the reason for enhancing the efficacy of the process [31,32].

Since there was no report for the application of SDS functionalized MNs to remove the benzene from the aqueous solution, we conducted this study by taking into consideration of different effective parameters, including pH, contact time, adsorbent dosage, initial benzene concentration, temperature, on the efficiency of the studied process. Moreover, similar to other adsorption studies, since the characterization of the studied adsorbent is important, it was also considered to determine using analyses such as scanning electron microscopy (SEM), X-ray diffraction (XRD), Fourier-transform infrared spectroscopy (FTIR), and Brunauer–Emmett–Teller (BET). In addition, isotherm, kinetic and thermodynamic studies for adsorption of benzene by our prepared adsorbent were done.

2. Material and methods

2.1. Chemical and reagents

Benzene, ferric chloride ($FeCl_3{\cdot}6H_2O$), ferrous chloride ($FeCl_2{\cdot}4H_2O$), sodium hydroxide, sodium dodecyl sulfate (SDS), acetic acid, and hydrochloric acid were the chemicals used in the present study, which were provided by Merck (Darmstadt, Germany). Preparing stock solution was done by dissolving a known amount of benzene in distilled water.

2.2. Synthesis of MNPs

Synthesizing MNPs was done based on the co-precipitation method reported in other studies [25]. First, 2 g of iron(II) and iron(III) salts were mixed and dissolved in 200 mL of double-distilled water in a 1,000 mL three-necked balloon as sources of production of iron(II) and iron(III) ions. Then, using a mechanical stirrer, the solution was stirred under argon gas for 15 min until the temperature reached 80°C. 120 mL of 1.5 M ammonia solution was then instilled into the solution and the stirring rate was raised. At this stage, the color of the solution changed from orange to black (In all stages of synthesis, a neutral atmosphere was used in a way that argon gas was continuously blown into the balloon and the initial solutions). After 30 min, litmus paper was inserted in a balloon opening and the pH of the solution vapor was measured, and when it reached 9, the addition of ammonia was stopped. The final volume of the solution is about 350 mL. After about 1.5 h of stirring the solution and its uniformity for 20 min, the stirring stopped and the resulting black precipitate was separated from the solution by magnetization and the remaining solution overflowed. To completely separate the ammonia and lower the pH to about 7, the washing operation was repeated several times with distilled water and then the nanoparticles were removed from the environment with a magnet and washed and dried three times.

Characterization of the prepared MNPs was done using the analyses methods including FTIR (VERTEX 70, Bruker Scientific Instruments Co., Germany), XRD ((Bruker Scientific

Instruments Co., Germany) using Cu-Kα radiation), SEM (Hitachi SU8020, Hitachi High-Tech Co., Ltd., Japan) and BET (Micromeritics Instrument Co., Norcross, GA, USA).

2.3. Experimental studies

To make the stock solution, 0.64 g of benzene was poured into a 500 mL volumetric flask and was brought to volume, and then stirred on a heater using a mechanical stirrer for 1 h. Finally, a solution of 1,000 mg/L benzene was prepared. To make other concentrations of benzene (10, 20, 40, 60, 80, and 100 mg/L), a stock solution was used with appropriate dilution ratios. In this study, a volume of 100 mL was considered for experiments. After drawing the standard curve, the experiment was started and all the samples tested in this study were synthetic samples. According to the specific objectives of the research to determine the effect of different parameters, the experiments were examined separately step by step to find the most suitable optimal point. Different doses of MNs/SDS (0.2, 0.4, 0.6, 0.8, and 1 g/L), benzene concentration (10, 20, 40, 60, 80, and 100 mg/L), contact times (10, 20, 30, 45, 60, 90, 120, and 150 min), different pH values (3, 5, 7, 9, and 11), and temperature (20°C, 30°C, 40°C, and 50°C) were tested. In this study, the optimal level of each variable (pH, magnetite nanoparticle dose, benzene concentration, and contact time) was determined. In other words, by changing one variable and keeping the other variables constant, the effect of the variables in removing benzene was studied. Finally, after performing all the steps of testing and extracting the samples for injection in gas chromatography, the final concentration (output) of benzene was read by the device.

GC device (model: Agilent 7890A, Palo Alto USA, CA) was utilized to measure the amount of benzene removed. The detector of this device was of FID type or flame ionization with an HP-5 capillary column with a length of 30 m and a thickness of 0.25 μm. The amount of benzene adsorbed on the adsorbent and its removal efficiency was calculated by the following equations [33,34]:

$$\%R = \frac{C_0 - C_e}{C_0} \times 100 \tag{1}$$

$$q_e = \left(\frac{C_0 - C_e}{M} \right) \times V \tag{2}$$

where C_0 and C_e are the initial concentration and equilibrium concentrations of benzene after adsorption. q_e is mg of benzene adsorbed on the adsorbent. M and V are the adsorbent mass (g) and the volume of solution (L), respectively.

3. Results and discussion

3.1. Characteristics of prepared adsorbent

The surface morphology of nanoparticles coated with sodium dodecyl sulfate was examined by scanning electron microscopy images. As shown in Fig. 1a, SDS-coated magnetite nanoparticles are uniformly polished and have a spherical shape. Fig. 1b shows the FTIR spectrum of magnetic nanoparticles before the adsorption of contaminants. As can be seen, the adsorption peak observed at 547 cm^{-1} is related to the stretching vibrations of Fe_3O_4 [32].

The X-ray diffraction pattern of magnetite nanoparticles (shown in Fig. 1c) indicates the consistency of all the diffraction with the six diffraction peaks at (220), (311), (400), (422), (511), and (440). It was concluded based on the comparison of observed peaks with the Joint Committee on Powder Diffraction Standards (JCPDS card, file No. 79-0418) and is representative of the cubic spinel phase of Fe_3O_4. Accordingly, considering the obtained XRD pattern, it is concluded that the prepared nanoparticles were Fe_3O_4 [31]. For estimating the average crystallite size (D in nm) of Fe_3O_4, the Scherer equation based on the following equation was employed [32].

$$D = \frac{K\lambda}{\beta \cos\theta} \tag{3}$$

where λ is used to represent the wavelength of the X-ray radiation (1.5406 Å), K is employed to show a constant taken as 0.89, θ is the diffraction angle, and β is the full width at half maximum. Using the mentioned equation, the average size of around 22 nm was found for the Fe_3O_4.

Specific surface area, which is frequently known as BET surface areas, were estimated based on the theory of BET to nitrogen adsorption/desorption isotherms measured at 77 K; according to the results of this analysis, MNs and MNs/SDS had the average specific surface areas of 91.2 and 83.4 m^2/g, respectively, which is representative of relatively larger specific surface areas for MNs. The possible aggregation after surface modification may be the reason for the decrease in the surface area of MNs/SDS [31].

3.2. Effect of studied parameters

The pH of the solution has been introduced to be one of the strategic and operative factors, which its study was also included in our work; its effect on the surface charge of adsorbent, ionization of material, and differentiation of functional groups of the adsorbent surface has provided this importance for this factor [35]. Accordingly, after regulating the pH of solutions at 3, 5, 7, 9, and 11, the benzene adsorption efficiency at each mentioned pH value was reported. The studies for determining the effect of this parameter were conducted using the constant values of other parameters (contact time = 60 min, MNs/SDS dosage = 0.6 g/L, benzene concentration = 10 mg/L, and temperature = 30°C). Based on reported efficiencies (Fig. 2a), the better removal efficiency was related to a pH of 7, which is in the neutral pH range. At the lower pH values, there are high concentrations of H^+, which have high mobility; this leads to rising competition between these ions with benzene molecules for adsorption sites and disrupting the adsorption process [36]. In addition, the reduction in efficiency was also detected for pH values greater than the neutral range. It is due to the occurrence of the competition between OH^- (produced in alkaline conditions) and benzene molecules for adsorption onto the available surface sites on the adsorbent [37]. According to

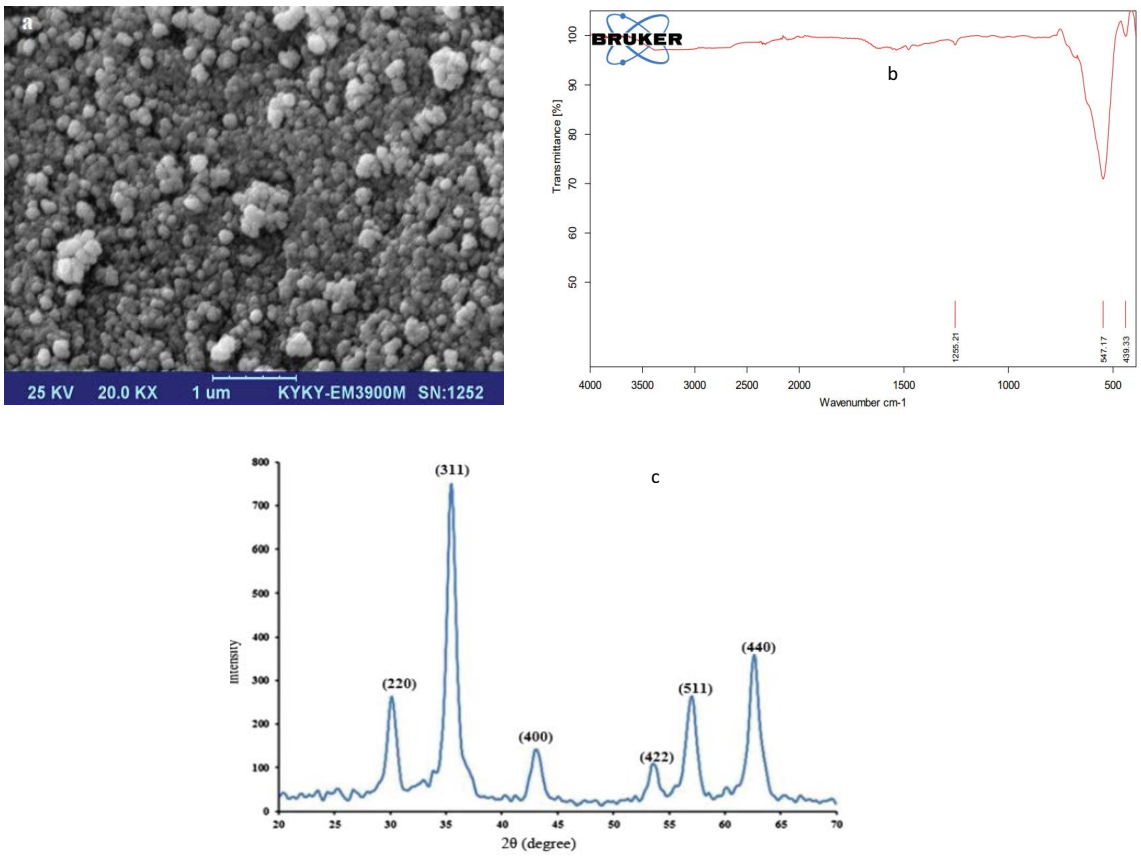

Fig. 1. SEM micrographs of MNs/SDS (a), FTIR pattern (b), XRD pattern of MNs/SDS (c).

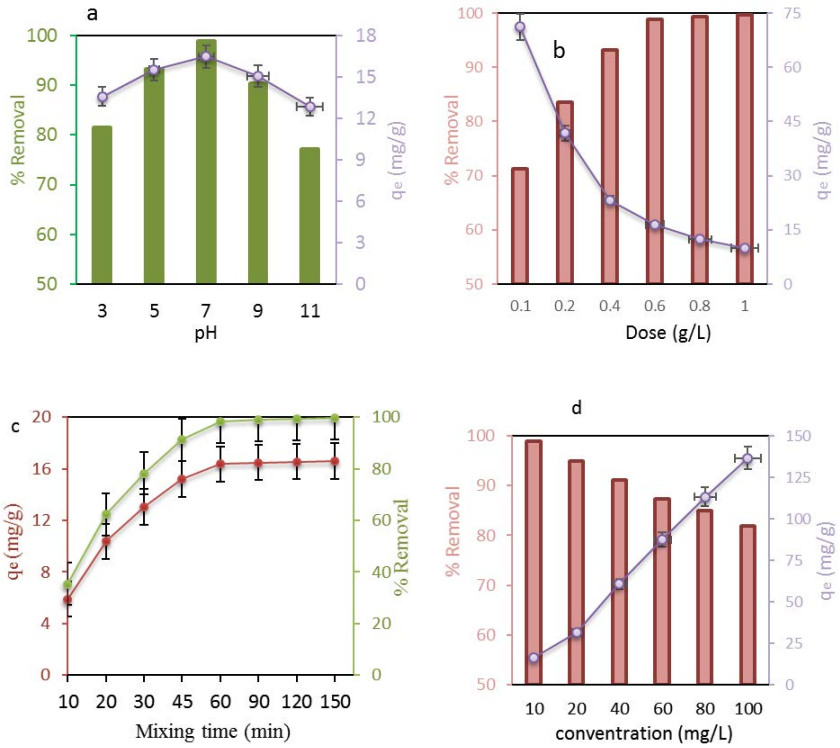

Fig. 2. Effect of pH (a), MNs/SDS dose (b), mixing time (c) and, concentration (d).

literature, surface polarity and hydrogen bonding between adsorbent and adsorbate may explain the lower adsorption efficiency in acidic and alkaline conditions [38].

MNs/SDS mass has also been reported to be an effective parameter in adsorption processes. The changes in the efficiency of the benzene adsorption by changes in the adsorbent dosages were determined at different adsorbent dosages of 0.1, 0.2, 0.4, 0.6, 0.8, and 1 g/L. The experiments of this part were conducted under constant values of other studied parameters, including contact time of 60 min, pH of 7, benzene concentration of 10 mg/L, and temperature of 30°C. As can be seen in Fig. 2b, which is related to the results of this part, an enhancement in removal efficiency from 71.2 to 99.4 was detected for increasing adsorbent dosage from 0.2 to 0.8 g/L. However, reverse results were observed for adsorption capacity so that it diminished from 71.2 to 9.97 mg/g when the adsorbent dosage changed from 0.2 to 1 g/L. In addition, at the adsorbent dosage of 0.6 mg/L, no enhancement could be detected in adsorption efficiency. To elucidate the development of adsorption efficiency by increasing the adsorbent, it should be considered that the number of the adsorbent sites for binding with the studied pollutant is increased and led to adsorbing more pollutant molecules by the adsorbent [39,40]. However, overlapping the adsorbent surfaces, which appears by increasing the adsorbent mass, has been mentioned as the reason for diminishing the adsorption capacity [41].

In the previous adsorption studies, the association between contact time and removal efficiency has been detected. Accordingly, for investigating the effect of this parameter in this study, the related experiments at the contact times, including 10, 20, 30, 45, 60, 90, 120, and 150 min, were conducted under optimum values obtained for other parameters (pH = 7, MNs/SDS mass = 0.6 g/L, benzene concentration = 10 mg/L, and temperature = 30°C). Fig. 2c represents results obtained from evaluating the effect of mentioned parameter on the adsorption efficiency. According to the results, the removal efficiency has developed by increasing the contact time up to 60 min, which is described by the provision of adequate time for necessary reactions (i.e., physical contact and chemical reaction). Most of the benzene was removed from the solution in the initial times. Explaining this event is done based on the higher accessibility of adsorption sites for pollutant molecules initially [42]. However, as time increase, appearing the repulsion force between pollutant molecules will be associated with the difficulty in occupying the remaining surface sites [43,44].

The initial concentration of benzene, as another effective parameter in the adsorption process, was evaluated using different concentrations of benzene, that is, 10, 20, 40, 60, 80, and 100 mg/L (Fig. 2d). Removal efficiencies observed for the studied concentrations exhibited the inverse effect of the studied parameter. Accordingly, removal efficiency has decreased so that it reached from 98.8% to 81.2% as the initial concentration of benzene increased from 10 to 100 mg/L. Since there is a limited active site for a certain amount of adsorbent, increasing the benzene concentration leads to saturation of the surface sites and a lack of enough sites for the adsorption of more pollutant molecules; this results in the removal efficiency [45,46]. Nonetheless, the adsorption capacity showed an increasing trend by increasing the initial concentration of pollutant and enhanced from 16.4 to 136.5 mg/g, which is enlightened by developing the driving force caused by a benzene concentration gradient [47].

3.3. Isotherm studies

This part of our studies was done to clarify the information, which is obtained by the isotherm models; this information includes adsorption mechanisms, adsorbent tendencies, and surface properties. There are different models utilized for this purpose [48–50]. The models used in the present study (along with their details) and the results obtained from these models have been brought in Table 1. The equilibrium data in both linear and nonlinear models follow the Langmuir isotherm. Fig. 3 shows the nonlinear models for the Freundlich, Langmuir, Temkin, and Dubinin–Radushkevich isotherms, and the Langmuir isotherm diagram is more in line with laboratory data and has more adaptation with the diagram of experimental results.

Also, Table 1 shows the results of linear isotherm models, and it can be seen that the regression coefficient for the Langmuir model is higher than other models.

The Q_{max} according to the Langmuir model at 20°C, 30°C, 40°C, and 50°C were 127, 131.2, 139.6, and 140.4 mg/g, respectively.

As known, the Langmuir model is employed for the stimulation of single-layer homogenous adsorption. However, using Freundlich isotherm models, the heterogeneous surface multi-phase adsorption is stimulated, and the interaction between solutes when sorbent adsorbs them is described by the Temkin isotherm model. Elucidation of the nature and type of the adsorption is performed using precise calculation of isotherm parameters [51]. According to constants obtained in our experimental conditions at the studied temperatures (B-Temkin: 0.0004, 0.0006, 0.0007, 0.0009 kJ/mol < 20 kJ/mol; *E*-energy: 4.41, 5.76, 7.11, and 7.84 kJ/mol < 8 kJ/mol), the adsorption was found to be physical, and the formation of weak van der Waals bonds on the MNs/SDS monolayer surface is detected. In addition, the equivalent binding sites could be perceived on MNs/SDS surface [52].

3.4. Kinetic studies

In Table 2, the kinetic models studied and results obtained from them have been represented. These models are used to express the adsorption mechanism and conformity of experimental data related to the adsorption of contaminants on adsorbents based on adsorption rate constants [53–55].

As can be seen in the results, the equilibrium data follow the linear and nonlinear pseudo-second-order kinetics models better than the pseudo-first-order and Elovich kinetic models. Fig. 4a shows the nonlinear model and its adaptation to the laboratory data, and as can be seen, the pseudo-second-order graph is exactly the same as the experimental data graph.

Table 2 also shows the results of the linear analysis of kinetics; it can be seen that the regression coefficient for

Table 1
Linear isotherm parameters for adsorption of benzene at various temperatures

Isotherm models	293 K	303 K	313 K	323 K
Langmuir: $\frac{1}{q_e}=\frac{1}{q_{max}}+\frac{1}{K_L C_e q_{max}}$, $R_L=\frac{1}{1+K_L C_0}$				
K_L = Langmuir isotherm constant (L/mg); Q_{max} = maximum monolayer coverage capacity (mg/g)				
q_m (mg/g)	127	131.2	139.6	140.4
K_L (L/mg)	0.0014	0.0019	0.0035	0.0049
R_L	0.877	0.841	0.741	0.671
R^2	0.991	0.994	0.992	0.998
Freundlich: $\log q_e=\frac{1}{n}\log C_e+\log K_F$				
q_e capacity adsorption (mg/g); K_F Freundlich indicator of adsorption capacity; $1/n$ intensity of the adsorption indicating the surface heterogeneity and favorability of the adsorption process				
K_F	3.17	5.25	6.89	7.27
$1/n$	0.746	0.573	0.527	0.412
R^2	0.941	0.901	0.892	0.879
Temkin: $q_e=B\ln K_T+B\ln C_e$				
B = Temkin isotherm constant related to the heat of adsorption J/mol; K_T is the Temkin isotherm equilibrium binding constant (L/g); R = universal gas constant (8.314 J/mol·K); T = absolute temperature in Kelvin				
K_T (L/g)	3.14	3.94	4.32	5.39
B (kJ/mol)	0.0004	0.00006	0.0007	0.0009
R^2	0.871	0.843	0.849	0.956
Dubinin–Radushkevich: $\log q_e=\ln q_m-\beta\varepsilon^2$, $\varepsilon=RT\ln\left[1+\frac{1}{C_e}\right]$				
q_m = theoretical adsorption isotherm saturation capacity (mg/g); β is the Dubinin–Radushkevich isotherm constant (mol²/kJ²); ε is Polanyi potential; E = average energy of adsorption kJ/mol				
q_m (mg/g)	69.2	78.4	83.1	90.2
E	4.41	5.76	7.11	7.84
R^2	0.911	0.892	0.904	0.873

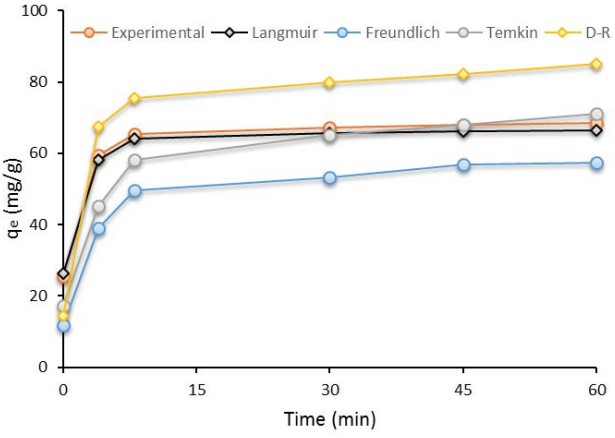

Fig. 3. Nonlinear adsorption isotherms for the adsorption of benzene onto MNs/SDS.

all concentrations for pseudo-second-order is better than pseudo-first-order and Elovich models, and the adsorption capacity obtained from pseudo-second-order is more in line with the experimental adsorption capacity.

To determine the mechanism of benzene adsorption by MNs/SDS, the intraparticle diffusion (IPD) kinetic model was used, and the results were represented in Fig. 4b; as can be seen, the graph of q_t against reaction time ($t^{1/2}$) shows a multi-step adsorption process.

The first step of the studied process was the quick occupancy of the MNs/SDS surface by benzene molecules due to the occurrence of surface adsorption due to the presence of brilliant active adsorption sites. By decreasing the available adsorption sites, which occurs due to occupying them with benzene gradually, the second adsorption step starts; it encompasses diffusion-driven adsorption into internal pores [56]. In the first step, as shown in Fig. 4b, the rapid benzene adsorption, which happens within a

Table 2
Linear kinetic parameters for the adsorption of benzene on MNs/SDS

Model	Parameters	10 mg/L	20	40	60	80	100
$q_{e,\exp}$	–	16.1	39.9	61.6	88.2	114.5	139.8
Pseudo-first-order: $\log(q_e - q_t) = \log q_e - \frac{K_1}{2.303} t$ (41)	$q_{e,\text{cal}}$	8.1	16.4	29.1	47.2	56.3	71.7
	K_1	0.012	0.024	0.045	0.068	0.073	0.084
q_e = adsorption capacity at equilibrium time; q_t = adsorption capacity at time t (mg/g); K_1 (min^{-1}) = equilibrium rate constant for pseudo-first-order	R^2	0.894	0.902	0.913	0887	0.872	0.885
Pseudo-second-order: $\frac{t}{q_t} = \frac{1}{K_2 q_e^2} + \frac{1}{q_e}$ (42)	$q_{e,\text{cal}}$	16.2	37.1	65.9	85.4	110.9	142.3
	K_2	0.0019	0.0024	0.0035	0.0033	0.0047	0.0061
K_2 (g/mg·min) = equilibrium rate constant for pseudo-second-order	R^2	0.999	0.998	0.993	0.997	0.999	0.992
Elovich: $q_t = \frac{1}{\beta}\ln(\alpha\beta) + \frac{1}{\beta}\ln(t)$ (43)	$q_{e,\text{cal}}$	10.2	18.4	26.9	39.5	48.2	61.5
	$\alpha \times 10^6$	1.69	2.51	3.26	3.77	3.95	4.69
	β	0.0024	0.0039	0.0071	0.011	0.029	0.042
q_t = amount of adsorbate/g adsorbent at time; α is the initial adsorption rate (mg/g·min); β is the desorption constant (g/mg)	R^2	0.845	0.891	0.887	0.914	0.927	0.945
	Stage 1						
	K_b	1.65	4.29	9.34	18.5	27.5	39.2
	C	3.08	6.59	16.2	27.1	38.8	44.2
	R^2	0.917	0.956	0.949	0.927	0.991	0..964
Intraparticle diffusion	Stage 2						
$q_t = K_b t^{1/2} + C$ (44)	K_b	1.02	1.95	4.27	9.19	14.6	19.5
K_b = Intraparticle diffusion rate constant (mg/g·$\text{min}^{1/2}$);	C	5.27	9.14	24.6	39.9	51.5	68.2
C = thickness of the boundary layer	R^2	0.914	0.926	0.973	0.969	0.947	0.958
	Stage 3						
	K_b	0.172	0.345	0.427	0.561	0.712	0.794
	C	9.25	17.2	39.4	56.2	79.3	99.2
	R^2	0.941	0.963	0.927	0.942	0.981	0.948

short period of time, is clear. The remained benzene in the first step was decreased and removed in the third step. The straight line does not cross the origin, so IPD is not the only rate-limiting step [57].

3.5. Effect of temperature and thermodynamic studies

In adsorption studies, acquiring better knowledge about the adsorption process is done using the thermodynamics of adsorption; in this study, it was done at temperature levels including 293, 303, 313, and 323 K. Van't Hoff equation is the utilized formula for determining thermodynamic limitations (i.e., Gibbs free energy variation (ΔG°), the enthalpy variation (ΔH°), and the entropy variation (ΔS°) [Eqs. (4)–(6)] [58–60]:

$$\Delta G^\circ = -RT\ln K \tag{4}$$

$$\ln K = \left(\frac{\Delta S^\circ}{R}\right) - \left(\frac{\Delta H^\circ}{RT}\right) \tag{5}$$

$$K = \frac{q_e}{C_e} \tag{6}$$

Using the results obtained from the slope and intercept of the lnK_c vs. 1/T plot, as well as the intercept of the Arrhenius plot, the standard enthalpy variation (ΔH°) and standard entropy variation (ΔS°) were determined. Since a positive value was obtained for ΔH° (44.2 kJ/mol), the adsorption process was endothermic. Negative ΔG° values (values –2.14, –4.02, –5.95, and 8.11 kJ/mol at temperatures of 293, 303, 313, and 323 K, respectively) indicate the spontaneous nature of the benzene on MNs/SDS. Based on our observations, the negativity of ΔG° increases as temperature rises, which leads to developing the "favorability" of (ΔG°) [61]. As mentioned, adsorbing the benzene onto MNs/SDS is an endothermic reaction, which may be explained by the greater mobility of benzene molecule and higher adsorbent molecule diffusion rates across MNs/SDS surfaces at higher temperatures; these events develop adsorption effectiveness [62]. A positive value of ΔS° (0.342 kJ/mol·K) indicates a random increase

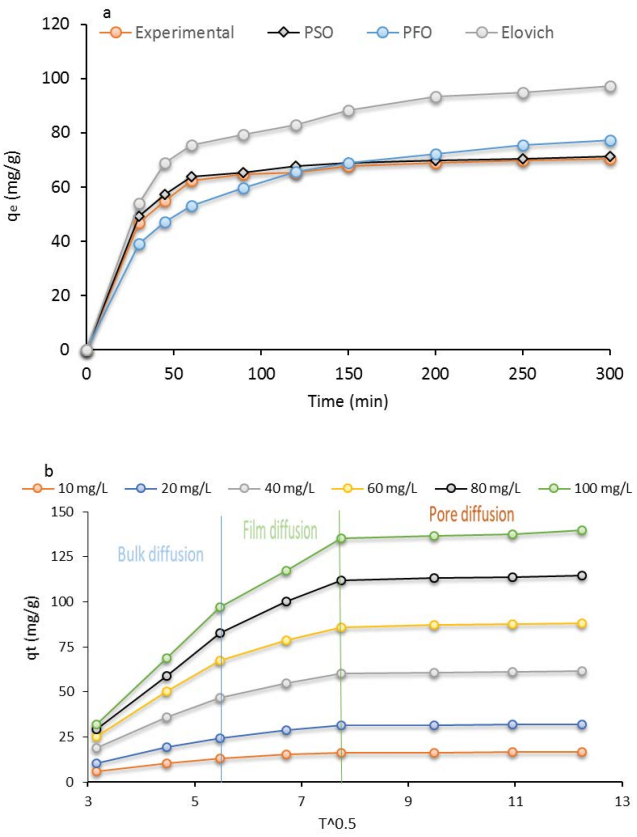

Fig. 4. Adsorption kinetics for benzene removal. Nonlinear kinetics (a) and intraparticle diffusion (b).

in the solid–liquid interface that points out the affinity between the benzene and the MNs/SDS [63].

4. Conclusion

In the present study, using the batch system, examining the efficacy of MNs/SDS was done to adsorb benzene. This study was conducted by focusing on the main factors having an effect on adsorption efficiency. The factors were concentration of target pollutants, pH of the solution, contact time, mass of MNs/SDS, and temperature. The optimal conditions for mentioned factors were concentration of 10 mg/L, pH of 3, mass of 0.6 g/L, and time of 60 min and temperature of 50°C; the process could offer removal efficiency of 100% under the above-mentioned conditions. The spontaneous and endothermic nature of the process was confirmed based on the obtained values for thermodynamic parameters. Linear and nonlinear models of kinetics and isotherms were calculated. The maximum adsorption capacity was 140.4 mg/g, and the Langmuir model exhibited a better fit for the isothermal data. The current study approved the ability of MNs/SDS as an efficient adsorbent for removing benzene (up to 100%).

Acknowledgements

The authors are grateful to the Zahedan University of Medical Sciences for the financial support of this study (Code project: 9663).

References

[1] O. Baytar, O. Şahin, C. Saka, S. Ağrak, Characterization of microwave and conventional heating on the pyrolysis of pistachio shells for the adsorption of methylene blue and iodine, Anal. Lett., 51 (2018) 2205–2220.
[2] D. Balarak, Y. Mahdavi, E. Bazrafshan, A.H. Mahvi, Kinetic, isotherms and thermodynamic modeling for adsorption of acid blue 92 from aqueous solution by modified *Azolla filiculoides*, Fresenius Environ. Bull., 25 (2016) 1321–1330.
[3] A.N. Nnaemeka. Environmental pollution and associated health hazards to host communities (case study: Niger delta region of Nigeria), Cent. Asian J. Environ. Sci. Technol. Innovation, 1 (2020) 30–42.
[4] A.B. Al-Hawash, M.A. Dragh, S. Li, A. Alhujaily, Principles of microbial degradation of petroleum hydrocarbons in the environment, Egypt. J. Aquat. Res., 44 (2018) 71–76.
[5] A. Adachi, H. Hamamoto, T. Okano, Use of lees materials as an adsorbent for removal of organochlorine compounds or benzene from wastewater, Chemosphere, 58 (2005) 817–822.
[6] P.M. Stähelin, A. Valério, Benzene and toluene removal from synthetic automotive gasoline by mono and bicomponent adsorption process, Fuel, 231 (2018) 45–52.
[7] M. Tang, X. Huang, Y. Peng, S. Lu, Hierarchical porous carbon as a highly efficient adsorbent for toluene and benzene, Fuel, 270 (2020) 117478, doi: 10.1016/j.fuel.2020.117478.
[8] D. Loomis, K.Z. Guyton, Y. Grosse, F. El Ghissassi, V. Bouvard, L. Benbrahim-Tallaa, N. Guha, N. Vilahur, H. Mattock, K. Straif, Carcinogenicity of benzene, Lancet Oncol., 18 (2017) 1574–1575.
[9] A. Sekar, G.K. Varghese, M.K. Ravi Varma, Analysis of benzene air quality standards, monitoring methods and concentrations in indoor and outdoor environment, Heliyon, 5 (2019) e02918, doi: 10.1016/j.heliyon.2019.e02918.
[10] W. Abplanalp, N. DeJarnett, D.W. Riggs, D.J. Conklin, J.P. McCracken, S. Srivastava, Z. Xie, S. Rai, A. Bhatnagar, T.E. O'Toole, Benzene exposure is associated with cardiovascular disease risk, PLoS One, 12 (2017) e0183602, doi: 10.1371/journal.pone.0183602.
[11] H.A. Maksoud, M.G. Elharrif, M.K. Mahfouz, M.A. Omnia, M.H. Abdullah, M.E. Eltabey, Biochemical study on occupational inhalation of benzene vapours in petrol station, Respir. Med. Case Rep., 27 (2019) 100836, doi: 10.1016/j.rmcr.2019.100836.
[12] R. Sun, K. Xu, Q. Zhang, X. Jiang, Z. Man, Plasma metabonomics investigation reveals involvement of fatty acid oxidation in hematotoxicity in Chinese benzene-exposed workers with low white blood cell count, Environ. Sci. Pollut. Res., 25 (2018) 32506–32514.
[13] H. Mohamed, M.A. Swani, M.I. Alaghib, A.I. Abdeljawad, M. Alkezza, M. Alobaidy, Hematological assessment of benzene exposure among employees in Brega Oil Marketing Company (BOMC), Benghazi. Int. Blood Res. Rev., 8 (2018) 1–7.
[14] B.D. Spycher, J.E. Lupatsch, A. Huss, J. Rischewski, Parental occupational exposure to benzene and the risk of childhood cancer: a census-based cohort study, Environ. Int., 108 (2017) 84–91.
[15] M. Talibov, J. Sormunen, J. Hansen, K. Kjaerheim, J.I. Martinsen, Benzene exposure at workplace and risk of colorectal cancer in four Nordic countries, Cancer Epidemiol., 55 (2018) 156–161.
[16] A. De Donno, M. De Giorgi, F. Bagordo, T. Grassi, A. Idolo, F. Serio, E. Ceretti, D. Feretti, M. Villarini, M. Moretti, A. Carducci, M. Verani, S. Bonetta, C. Pignata, S. Bonizzoni, A. Bonetti, U. Gelatti, MAPEC_LIFE Study Group, Health risk associated with exposure to PM10 and benzene in three Italian towns, Int. J. Environ. Res. Public Health, 15 (2018) 1672, doi: 10.3390/ijerph15081672.
[17] S.J. Varjani, E. Gnansounou, A. Pandey, Comprehensive review on toxicity of persistent organic pollutants from petroleum refinery waste and their degradation by microorganisms, Chemosphere, 188 (2017) 280–291.
[18] H. Huang, H. Huang, Q. Feng, G. Liu, Y. Zhan, M. Wu, Catalytic oxidation of benzene over Mn modified TiO_2/ZSM-5 under vacuum UV irradiation, Appl. Catal., B, 203 (2017) 870–878.

[19] H. Huang, G. Liu, Y. Zhan, Y. Xu, H. Lu, Photocatalytic oxidation of gaseous benzene under VUV irradiation over TiO_2/zeolites catalysts, Catal. Today, 281 (2017) 649–655.
[20] R. Rashid, I. Shafiq, P. Akhter, M.J. Iqbal, M. Hussain, A state-of-the-art review on wastewater treatment techniques: the effectiveness of adsorption method, Environ. Sci. Pollut. Res., 28 (2021) 9050–9066.
[21] Q. Yang, X. Wang, W. Luo, J. Sun, Q. Xu, F. Chen, Effectiveness and mechanisms of phosphate adsorption on iron-modified biochars derived from waste activated sludge, Bioresour. Technol., 247 (2018) 537–544.
[22] G.I. Danmaliki, T.A. Saleh, A.A. Shamsuddeen, Response surface methodology optimization of adsorptive desulfurization on nickel/activated carbon, Chem. Eng. J., 313 (2017) 993–1003.
[23] M.A. Islam, M. Ahmed, W. Khanday, M. Asif, B. Hameed, Mesoporous activated carbon prepared from NaOH activation of rattan (*Lacosperma secundiflorum*) hydrochar for methylene blue removal, Ecotoxicol. Environ. Saf., 138 (2017) 279–285.
[24] L. Mohammed, H.G. Gomaa, D. Ragab, J. Zhu, Magnetic nanoparticles for environmental and biomedical applications: a review, Particuology, 30 (2017) 1–14.
[25] S. Liu, B. Yu, S. Wang, Y. Shen, H Cong, Preparation, surface functionalization and application of Fe_3O_4 magnetic nanoparticles, Adv. Colloid Interface Sci., 281 (2020) 102165, doi: 10.1016/j.cis.2020.102165.
[26] M.Ş. Ece, A. Ekinci, S. Kutluay, Facile synthesis and comprehensive characterization of Ni-decorated amine groups-immobilized Fe_3O_4@SiO_2 magnetic nanoparticles having enhanced solar cell efficiency, J. Mater. Sci.: Mater. Electron., 32 (2021) 18192–18204.
[27] S. Kutluay, O. Şahin, M.S. Ece, Fabrication and characterization of Fe_3O_4/perlite, Fe_3O_4/perlite@SiO_2, and Fe_3O_4/perlite@SiO_2@sulfanilamide magnetic nanomaterials, Appl. Phys. A, 128 (2022) 222–231.
[28] S. Kutluay, S. Horoz, O. Şahin, M.S. Ece, Highly improved solar cell efficiency of Mn-doped amine groups-functionalized magnetic Fe_3O_4@SiO_2 nanomaterial, Energy Res., 45 (2021) 20176–20185.
[29] X. Yu, H. Yang, Pyrethroid residue determination in organic and conventional vegetables using liquid-solid extraction coupled with magnetic solid phase extraction based on polystyrene-coated magnetic nanoparticles, Food Chem., 217 (2017) 303–310.
[30] M. Abedi, M. Ahmadmoazzam, N. Jaafarzadeh, Removal of cationic tolonium chloride dye using Fe_3O_4 nanoparticles modified with sodium dodecyl sulfate, Chem. Biochem. Eng. Q., 32 (2018) 205–213.
[31] S. Shariati, M. Faraji, Y. Yamini, A.A. Rajabi, Fe_3O_4 magnetic nanoparticles modified with sodium dodecyl sulfate for removal of safranin O dye from aqueous solutions, Desalination, 270 (2011) 160–165.
[32] C. Muthukumaran, V.M. Sivakumar, S. Sumathi, M. Thirumarimurugan, Adsorptive removal of recalcitrant auramine-O dye by sodium dodecyl sulfate functionalized magnetite nanoparticles: isotherm, kinetics, and fixed-bed column studies, Int. J. Nanosci., 19 (2020) 1950004, doi: 10.1142/S0219581X19500042.
[33] F. Talebzadeh, S. Sobhanardakani, R. Zandipak, Effective adsorption of As(V) and V(V) ions from water samples using 2,4-dinitrophenylhydrazine functionalized sodium dodecyl sulfate-coated magnetite nanoparticles, Sep. Sci. Technol., 52 (2017) 622–633.
[34] Y. Fan, C. Zheng, H. Liu, C. He, Z. Shen, Effect of pH on the adsorption of arsenic(V) and antimony(V) by the black soil in three systems: performance and mechanism, Ecotoxicol. Environ. Saf., 191 (2020) 110145, doi: 10.1016/j.ecoenv.2019.110145.
[35] H. Anjum, K. Johari, N. Gnanasundaram, A. Appusamy, M. Thanabalan, Investigation of green functionalization of multiwall carbon nanotubes and its application in adsorption of benzene, toluene & p-xylene from aqueous solution, J. Cleaner Prod., 221 (2019) 323–338.
[36] M.M. Amin, B. Bina, A.M.S. Majd, Benzene removal by nano magnetic particles under continuous condition from aqueous solutions, Front. Environ. Sci. Eng., 8 (2014) 345–356.
[37] J.S. Costa, E.G. Bertizzolo, D. Bianchini, A.R. Fajardo, Adsorption of benzene and toluene from aqueous solution using a composite hydrogel of alginate-grafted with mesoporous silica, J. Hazard. Mater., 418 (2021) 126405, doi: 10.1016/j.jhazmat.2021.126405.
[38] H. Pourzamani, Y. Hajizadeh, S. Fadaei, Efficiency enhancement of multi-walled carbon nanotubes by ozone for benzene removal from aqueous solution, Int. J. Environ. Health Eng., 4 (2015) 29–38.
[39] B.A. Abussaud, Synthesis, characterization and application of carbon nanotubes decorated with zinc oxide nanoparticles for removal of benzene, toluene and p-xylene from aqueous solution, Sustainability, 13 (2021) 11716, doi: 10.3390/su132111716.
[40] T.J. Al-Musawi, G. McKay, A. Kadhim, M.M. Joybari, Activated carbon prepared from hazelnut shell waste and magnetized by Fe_3O_4 nanoparticles for highly efficient adsorption of fluoride, Biomass Convers. Biorefin., (2022) 1–16, doi: 10.1007/s13399-022-02593-z.
[41] D. Balarak, H. Abasizadeh, J.K. Yang, M.J. Shim, S.M. Lee, Biosorption of acid orange 7 (AO7) dye by canola waste: equilibrium, kinetic and thermodynamics studies, Desal. Water Treat., 190 (2021) 230, 331–339.
[42] J. Akpa, C. Nmegbu, Adsorption of benzene on activated carbon from agricultural waste materials, Res. J. Chem. Sci., 4 (2014) 34–40.
[43] A.D. Khatibi, A.H. Mahvi, N. Mengelizadeh, D. Balarak, Adsorption–desorption of tetracycline onto molecularly imprinted polymer: isotherm, kinetics, and thermodynamics studies, Desal. Water Treat., 230 (2021) 240–251.
[44] S. Kutluay, O. Baytar, O. Şahin, Equilibrium, kinetic and thermodynamic studies for dynamic adsorption of benzene in gas phase onto activated carbon produced from *Elaeagnus angustifolia* seeds, J. Environ. Chem. Eng., 7 (2019) 102947, doi: 10.1016/j.jece.2019.102947.
[45] T.J. Al-Musawi, N. Mengelizadeh, F. Ganji, C. Wang, D. Balarak, Preparation of multi-walled carbon nanotubes coated with $CoFe_2O_4$ nanoparticles and their adsorption performance for Bisphenol A compound, Adv. Powder Technol., 33 (2022) 103438, doi: 10.1016/j.apt.2022.103438.
[46] M.T. Raad, H. Behnejad, M.E. Jamal, Equilibrium and kinetic studies for the adsorption of benzene and toluene by graphene nanosheets: a comparison with carbon nanotubes, Surf. Interface Anal., 48 (2016) 117–125.
[47] R.A. Dyanati-Tilaki, Z. Yousefi, J. Yazdani-Cherati, The ability of *Azolla* and *Lemna minor* biomass for adsorption of phenol from aqueous solutions, J. Mazand. Univ. Med. Sci., 23 (2013) 140–146.
[48] M.I. Konggidinata, B. Chao, Q. Lian, R. Subramaniam, M. Zappi, Equilibrium, kinetic and thermodynamic studies for adsorption of BTEX onto ordered mesoporous carbon (OMC), J. Hazard. Mater., 336 (2017) 249–259.
[49] R.A. Diyanati, Z. Yousefi, J.Y. Cherati, Investigating phenol absorption from aqueous solution by dried *Azolla*, J. Mazand. Univ. Med. Sci., 22 (2013) 13–21.
[50] E. Batur, O. Baytar, S. Kutluay, S. Horoz, O. Şahin, A comprehensive new study on the removal of Pb(II) from aqueous solution by şırnak coal-derived char, Environ. Technol., 42 (2021) 1–14.
[51] E. Batur, S. Kutluay, Dynamic adsorption behavior of benzene, toluene, and xylene VOCs in single- and multi-component systems by activated carbon derived from defatted black cumin (*Nigella sativa* L.) biowaste, J. Environ. Chem. Eng., 10 (2022) 107565, doi: 10.1016/j.jece.2022.107565.
[52] M. Şakir Ece, S. Kutluay, Comparative and competitive adsorption of gaseous toluene, ethylbenzene, and xylene onto natural cellulose-modified Fe_3O_4 nanoparticles, J. Environ. Chem. Eng., 10 (2022) 107389, doi: 10.1016/j.jece.2022.107389.
[53] S. Kutluay, Excellent adsorptive performance of novel magnetic nano-adsorbent functionalized with 8-hydroxyquinoline-5-sulfonic acid for the removal of volatile organic compounds (BTX) vapors, Fuel, 287 (2021) 119691, doi: 10.1016/j.fuel.2020.119691.

[54] N. Genli, S. Kutluay, O. Şahin, Preparation and characterization of activated carbon from hydrochar by hydrothermal carbonization of chickpea stem: an application in methylene blue removal by RSM optimization, Int. J. Phytorem., 24 (2022) 1–11.
[55] A. Meshkinain, B. Davoud, Y. Nastaran, Optimization of nickel oxide nanoparticle synthesis through the sol-gel method for adsorption of Penicillin G, Res. J. Chem. Environ., 25 (2021) 31–36.
[56] H. Azarpira, Y. Mahdavi, O. Khaleghi, D. Balarak, Thermodynamic studies on the removal of metronidazole antibiotic by multi-walled carbon nanotubes, Pharm. Lett., 8 (2016) 107–113.
[57] M. Sillanpää, A.H. Mahvi, D. Balarak, A.D. Khatibi, Adsorption of acid orange 7 dyes from aqueous solution using polypyrrole/nanosilica composite: experimental and modelling, Int. J. Environ. Anal. Chem., (2021), doi: 10.1080/03067319.2020.1855338.
[58] T.J. Al-Musawi, N. Mengelizade, O. Al Rawi, D. Balarak, Capacity and modeling of acid blue 113 dye adsorption onto chitosan magnetized by Fe_2O_3 nanoparticles, J. Polym. Environ., 30 (2022) 344–359.
[59] T.J. Al-Musawi, N. Mengelizade, M. Taghavi, S. Mohebi, D. Balarak, Activated carbon derived from *Azolla filiculoides* fern: a high-adsorption-capacity adsorbent for residual ampicillin in pharmaceutical wastewater, Biomass Convers. Biorefin., (2021), doi: 10.1007/s13399-021-01962-4.
[60] D. Balarak, M. Baniasadi, S.M. Lee, M.J. Shim, Ciprofloxacin adsorption onto *Azolla filiculoides* activated carbon from aqueous solutions, Desal. Water Treat., 218 (2021) 444–453.
[61] T.J. Al-Musawi, A.H. Mahvi, A.D. Khatibi, Effective adsorption of ciprofloxacin antibiotic using powdered activated carbon magnetized by iron(III) oxide magnetic nanoparticles, J. Porous Mater., 28 (2021) 835–852.
[62] D. Balarak, Z. Taheri, M.J. Shim, S.-M. Lee, C. Jeon, Adsorption kinetics and thermodynamics and equilibrium of ibuprofen from aqueous solutions by activated carbon prepared from *Lemna minor*, Desal. Water Treat., 215 (2021) 183–193.
[63] D. Balarak, A.H. Mahvi, M.J. Shim, S.M. Lee, Adsorption of ciprofloxacin from aqueous solution onto synthesized NiO: isotherm, kinetic and thermodynamic studies, Desal. Water Treat., 212 (2021) 390–400.